

Crystals of Janus colloids at various interaction ranges

Z. Preisler, T. Vissers, F. Smallenburg, and F. Sciortino

Citation: *J. Chem. Phys.* **145**, 064513 (2016); doi: 10.1063/1.4960423

View online: <http://dx.doi.org/10.1063/1.4960423>

View Table of Contents: <http://aip.scitation.org/toc/jcp/145/6>

Published by the [American Institute of Physics](#)

Crystals of Janus colloids at various interaction ranges

Z. Preisler,^{1,2} T. Vissers,^{1,3} F. Smallenburg,^{1,4} and F. Sciortino¹

¹*Dipartimento di Fisica, Università di Roma "Sapienza," Piazzale Aldo Moro 5, 00185 Roma, Italy*

²*Soft Condensed Matter, Debye Institute for Nanomaterials Science, Utrecht University, Princetonplein 5, 3584 CC Utrecht, The Netherlands*

³*SUPA and School of Physics and Astronomy, The University of Edinburgh, James Clerk Maxwell Building, Peter Guthrie Tait Road, Edinburgh EH9 3FD, United Kingdom*

⁴*Institut für Theoretische Physik II: Weiche Materie, Heinrich-Heine-Universität Düsseldorf, Universitätsstr. 1, 40225 Düsseldorf, Germany*

(Received 23 April 2016; accepted 24 July 2016; published online 11 August 2016)

We investigate the effect of interaction range on the phase behaviour of Janus particles with a Kern-Frenkel potential. Specifically, we study interaction ranges $\Delta = 0.1\sigma, 0.3\sigma, 0.4\sigma, 0.5\sigma$ with σ the particle diameter, and use variable box shape simulations to predict crystal structures. We found that changing the interaction range beyond 0.2σ drastically increases the variety of possible crystal structures. In addition to close-packed structures, we find body-centered tetragonal and AA-stacked hexagonal crystals, as well as several lamellar crystals. For long interaction ranges and low temperatures, we also observe an extremely large number of metastable structures which compete with the thermodynamically stable ones. These competing structures hinder the detection of the lowest-energy crystal structures, and are also likely to interfere with the spontaneous formation of the ground-state structure. Finally, we determine the gas-liquid coexistence curves for several interaction ranges, and observe that these are metastable with respect to crystallization. *Published by AIP Publishing.* [<http://dx.doi.org/10.1063/1.4960423>]

I. INTRODUCTION

One of the most versatile ways of tuning the phase behaviour of spherical colloidal particles is to decorate their surface with attractive patches. Experimentally, patchy particles can be synthesized in a variety of ways,^{1–5} and are used in the self-assembly of novel materials both by tuning their thermodynamic properties,^{3,6–11} as well as by controlling and exploiting their nonequilibrium behaviour.^{1,12} Even in thermodynamic equilibrium, patchy particles show a rich and complex phase behaviour, including a wide variety of stable crystal structures.^{13–16} This phase behaviour is controlled by the vast parameter space that defines the playing field. In particular, the number of patches per particle,^{13,16} patch size,^{17–19} patch shape,¹⁵ and interaction range^{13,20,21} have all been shown to play an important role in the phase behaviour. For example, similar to systems with isotropic attractive potentials,^{22–25} the gas-liquid coexistence can become metastable with respect to the fluid-crystal coexistence upon decreasing the range of the patchy attractions.²¹

The rich phase behaviour of patchy particles is exemplified by the simple case of a single patch per particle. One-patch spherical colloids, for which a number of experimental realizations have been developed,^{2–5,26,27} have drawn a considerable amount of theoretical attention, and have been predicted to spontaneously form many interesting structures. For example, computer simulations have shown that one-patch particles with a patch coverage fraction of 30% can form tube-like structures,^{28–30} while Janus particles (where exactly 50% of the particle surface is attractive) can form

micelles, vesicles, bilayers, and multiple crystal structures.¹⁴ Another recent simulation study demonstrated that tuning the patch coverage fraction of one-patch particles can further increase the number of accessible crystal structures.³¹

In this work, we investigate how the phase behaviour of Janus particles (with 50% surface coverage) changes upon altering the interaction range Δ , which sets the number and type of geometries in which the particles can bond with each other. We cover a large set of parameters for spherical one-patch particles modelled using the Kern-Frenkel potential,^{32,33} with interaction ranges up to 50% of the particle diameter σ . Snapshots of particles of the studied ranges with their bonding volumes are shown in Fig. 1. For these, we thoroughly investigate the phase behaviour by first identifying possible crystal structures and subsequently calculating the full equilibrium phase diagrams by means of free energy calculations and thermodynamic integration methods. Previous work on the crystal phases of Janus particles using this model focused on the cases $\Delta = 0.05\sigma$ ³¹ and $\Delta = 0.2\sigma$.¹⁴ Combining our new results with the phase diagrams from these studies provides a complete picture of the dependence of the phase diagram on the interaction range. Our results show that up to $\Delta \approx 0.2$ the phase diagram remains similar, mostly containing the same set of stable crystal structures, as the short interaction range limits bond formation to nearest neighbours only. Upon further increasing Δ , the number of possible stable crystals increases drastically, leading to a larger variety of crystal structures. For several interaction ranges, we also incorporate calculations of the gas-liquid phase separation and discuss its relative position with respect to the stability field of the crystals.

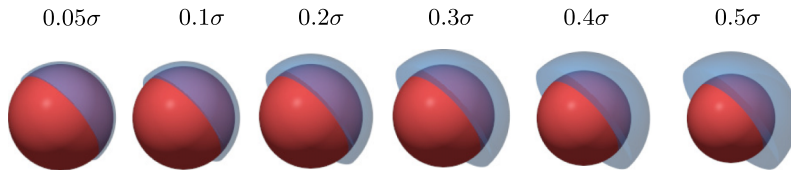


FIG. 1. Janus particles for six different values of the interaction range ($\Delta = 0.05\sigma, 0.1\sigma, 0.2\sigma, 0.3\sigma, 0.4\sigma,$ and 0.5σ). In the pictures the hard sphere particles are coloured in red and the bonding volume is depicted with transparent blue.

II. MODEL

In this work, we model the interactions between our Janus particles with a Kern-Frenkel potential u^{KF} , which is defined as^{32,33}

$$u^{\text{KF}}(\mathbf{r}_{ij}, \hat{\mathbf{n}}_i, \hat{\mathbf{n}}_j) = u^{\text{SW}}(r_{ij})\Omega(\hat{\mathbf{r}}_{ij}, \hat{\mathbf{n}}_i, \hat{\mathbf{n}}_j) + u^{\text{HS}}(r_{ij}), \quad (1)$$

where $u^{\text{SW}}(r_{ij})$ is a square-well interaction potential

$$u^{\text{SW}}(r_{ij}) = \begin{cases} -\epsilon & \text{if } \sigma < r_{ij} \leq \sigma + \Delta \\ 0 & \text{if } r_{ij} > \sigma + \Delta \end{cases} \quad (2)$$

and $\Omega(\hat{\mathbf{r}}_{ij}, \hat{\mathbf{n}}_i, \hat{\mathbf{n}}_j)$ is a function depending on the orientations of two interacting particles,

$$\Omega(\hat{\mathbf{r}}_{ij}, \hat{\mathbf{n}}_i, \hat{\mathbf{n}}_j) = \begin{cases} 1 & \text{if } \begin{cases} \hat{\mathbf{r}}_{ij} \cdot \hat{\mathbf{n}}_i > \cos \theta & \text{and} \\ \hat{\mathbf{r}}_{ji} \cdot \hat{\mathbf{n}}_j > \cos \theta \end{cases} \\ 0 & \text{otherwise} \end{cases} \quad (3)$$

Here \mathbf{r}_{ij} is a vector between particles i and j , r_{ij} is its length and $\hat{\mathbf{r}}_{ij}$ is the unit vector in the direction of \mathbf{r}_{ij} . $\hat{\mathbf{n}}_{i,j}$ denotes the orientations of the particles i, j . The diameter of the particles is denoted by σ , the interaction range Δ . Finally, the choice of the hard-sphere potential u^{HS} guarantees that the particles do not overlap

$$u^{\text{HS}}(r_{ij}) = \begin{cases} \infty & \text{if } r_{ij} \leq \sigma, \\ 0 & \text{otherwise.} \end{cases} \quad (4)$$

We choose $\cos \theta = 0$ to ensure that the patch surface coverage fraction of the Janus particles is exactly 50%. To illustrate, Fig. 2 shows a schematic representation of two Janus particles interacting via the potential in Eq. (1). The well depth ϵ fixes the energy scale, so that T is measured in units of ϵ/k_B , where k_B denotes the Boltzmann constant. Note that in an experimental setting, the effective temperature $k_B T/\epsilon$ can typically be tuned over a wide range, either by modifying the actual temperature or by modifying the interaction strength.

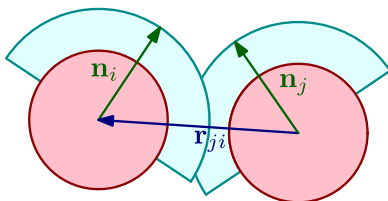


FIG. 2. Schematic representation of two spherical Janus colloids interacting with a Kern-Frenkel potential Eq. (1). The particles themselves are shown in pink, and the attractive bonding volumes are indicated in blue. The vector \mathbf{r}_{ij} points from the center of particle i to the center of particle j . The vectors $\hat{\mathbf{n}}_i$ and $\hat{\mathbf{n}}_j$ denote the orientations of particles i and j .

Finally, we remark that while it is possible with this interaction potential to reasonably reproduce the physical behaviour of colloids with short-ranged attractions, e.g., particles with one hydrophobic and one hydrophilic hemisphere,⁷ potentials with longer interaction lengths, especially at higher densities, may require many-body effects^{34–36} or more a more complex dependence on the interparticle distance or angular alignment between the particles. These effects are not included in the present potential choice, and may limit the ability of the model to quantitatively reproduce experimental situations.

III. METHODS

In order to determine the equilibrium phase diagrams for the systems under investigation, we use Monte Carlo computer simulations to calculate free energies of all competing phases, following the methodology described in Refs. 37 and 14. In particular, for each system we start our investigation by identifying candidate crystal structures using variable box shape or “floppy box” simulations.^{14,38,39} A small number of additional candidate structures were obtained from simulations where crystals spontaneously transform into a different structure. The different crystal structures are distinguished using various methods and order parameters described in Ref. 14. Subsequently, we calculate the free energy as a function of temperature and density in each phase (including the fluid) using thermodynamic integration techniques.³⁷ We determine coexistences from the calculated free energies by locating pairs of state points with equal pressure, temperature, and chemical potential. Phase coexistence lines are then traced out by using the Kofke integration method⁴⁰ starting from the identified coexistence points. In addition, gas-liquid coexistences and critical points were located using the successive umbrella sampling technique.⁴¹

IV. JANUS PARTICLES WITH $\Delta = 0.05\sigma$ TO 0.2σ

First, we investigate Janus colloids with interaction range $\Delta = 0.1\sigma$. Such short-ranged potentials are most close to experimental colloidal systems that exploit hydrophobic and hydrophilic interactions to create patchiness.^{8,42–44} The phase diagrams for $\Delta = 0.1\sigma$ in the T - p and ρ - T plane are shown in Fig. 3(a) and Fig. 3(b), respectively. Compared to the phase diagram for $\Delta = 0.05\sigma$, which was already calculated in Ref. 31, the phase diagram for $\Delta = 0.1\sigma$ has the same topology and contains the same stable crystal structures, although the coexistence densities are slightly different.

Our calculations reveal an equilibrium phase diagram containing three distinct crystal structures, indicated as **I**, **II**, and **W** (see Table I), as well as a fluid phase. At low densities and sufficiently high temperatures the fluid phase

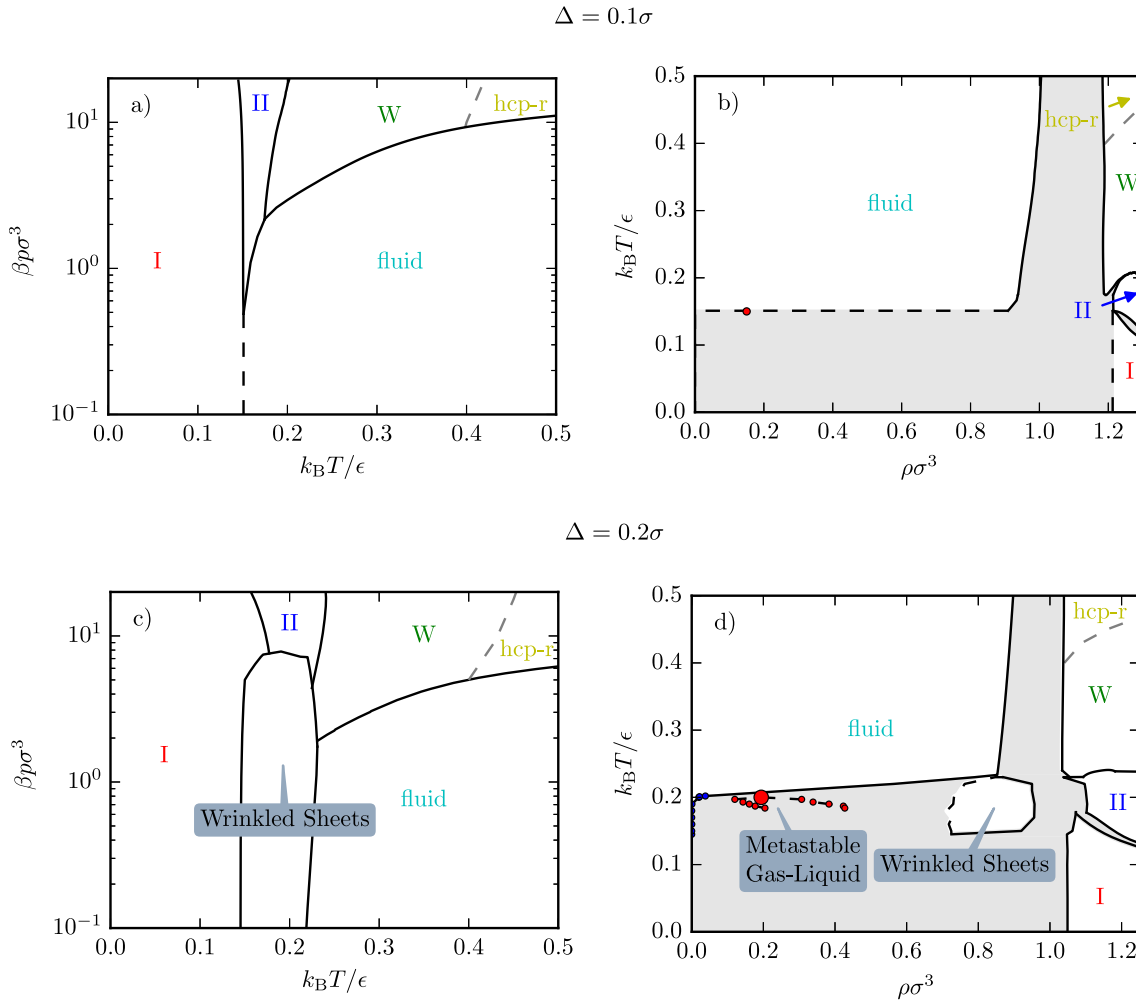


FIG. 3. Phase diagram of Janus particles in the T - p plane and in the ρ - T plane for interaction range $\Delta = 0.1\sigma$ (a) and (b), and $\Delta = 0.2\sigma$ (c) and (d). We identified stable phases **I**, **II**, **W** and the fluid, and wrinkled bilayer sheets (for $\Delta = 0.2\sigma$). The gas-liquid critical point and the gas-liquid coexistence are marked by red dots. Note that the critical point is metastable with respect to the crystal-gas coexistence for both interaction ranges. The dashed lines in (a) and (b) represent estimates of the fluid-crystal coexistence lines. Data for $\Delta = 0.2\sigma$ are reproduced with permission from J. Chem. Phys. **138**, 164505 (2013). Copyright 2013 AIP Publishing LLC.

is stable, as expected. At lower temperatures a low-density fluid coexists with crystal phases at high density. The crystal which is stable at the lowest temperatures is crystal **I**. In this structure, the particles are arranged in a face-centered cubic (fcc) lattice, where each particle is bonded to at most 9 neighbours (see Fig. 4(a)), resulting in an average number of 4.5 bonds per particle. Going up in temperature, crystal **II** becomes stable. In this phase, the particles are instead ordered on a hexagonally close-packed (hcp) lattice, with an average of 4.25 bonds per particle in the fully bonded

state (see Fig. 4(b)). Upon increasing the temperature even further, we find the **W** crystal, which again corresponds to a hcp-ordering of the particles, but with a significantly more complex bonding pattern (see Fig. 4(c)). When the temperature is increased even further the particle orientations become uncorrelated, which is indicated with a gray dashed line in Fig. 3.

For completeness, we also include the phase diagrams for $\Delta = 0.2\sigma$ from Ref. 14 in Figs. 3(c) and 3(d). For this interaction range, the same three crystal structures are stable, as well as one additional phase. The crystal structures at $\Delta = 0.2\sigma$ tend to form at lower densities, as the longer bonds allow for larger interparticle distances while retaining the same number of bonds.

Interestingly, the additional phase observed for $\Delta = 0.2\sigma$ is a peculiar stable crystal structure in the form of wrinkled bilayer sheets¹⁴ (see Fig. 4(d)). This structure does not appear in the phase diagram for ranges $\Delta \leq 0.1\sigma$. Indeed, our calculations show that on decreasing the range below $\Delta = 0.2\sigma$, particles can no longer form a sufficient amount of bonds to stabilize the structure. To assert at which interaction

TABLE I. List of crystal phases for an interaction range of $\Delta = 0.1\sigma$ displaying $U/N\epsilon$ and $\rho\sigma^3$ for selected $k_B T/\epsilon$, $\beta p\sigma^3$.

$\Delta = 0.1\sigma$				
Phase	$k_B T/\epsilon$	$\beta p\sigma^3$	$U/N\epsilon$	$\rho\sigma^3$
I	0.1	20	-4.5	1.23
II	0.17	11.8	-3.73	1.23
W	0.22	9.1	-3.27	1.21

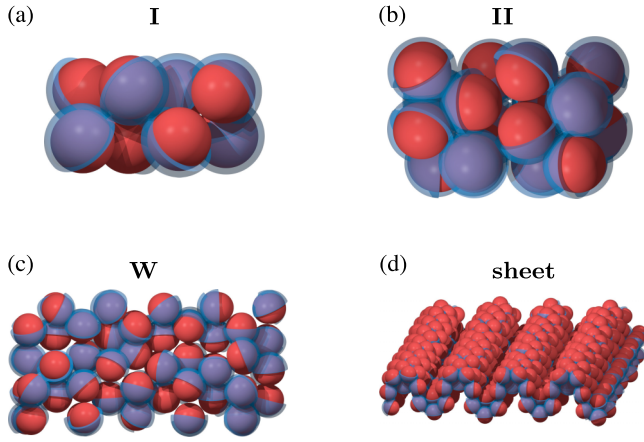


FIG. 4. Picture of crystal I, II, and W, the thermodynamically stable crystals found for the short interaction ranges $\Delta = 0.05\sigma$ and $\Delta = 0.2\sigma$. The picture also shows the wrinkled bilayer sheets (only one sheet shown), a stable structure for $\Delta = 0.2\sigma$. Reprinted with permission from J. Chem. Phys. **138**, 164505 (2013). Copyright 2013 AIP Publishing LLC.

range the wrinkled bilayer sheet breaks down, we performed simulations for $\epsilon \gg k_B T$ and $\Delta = 0.2\sigma$, starting from the wrinkled sheet phase, and decreased Δ at constant pressure and temperature (NpT). After each step, we allowed the configuration to equilibrate to reconnect bonds that were broken during the decrement of the interaction range. Using the above approach, we observe that the bilayer sheets can still exist down to an interaction range of $\Delta \approx 0.12\sigma$. For interaction ranges $\Delta < 0.12\sigma$ the network of bonds is broken and the structure falls apart.

In addition to the crystal phases, we calculated the gas-liquid critical point using successive umbrella sampling.⁴¹ In the phase diagram Fig. 3(b) we can see that for $\Delta = 0.1\sigma$ the critical point is metastable with respect to the gas-crystal coexistence, similar to what was previously found for $\Delta = 0.2\sigma$ (Fig. 3(d)). However, for $\Delta = 0.1\sigma$ the critical point is metastable with respect to the fluid-crystal coexistence with crystal W instead of the wrinkled bilayer sheets. We note that for range $\Delta = 0.2\sigma$ the critical point would have been stable if the wrinkled bilayer sheet phase had been absent. We also would like to draw attention to the peculiar shape of the gas-liquid metastable coexistence, displaying a re-entrant gas phase upon cooling, which originates from the onset of clustering in the gas phase.⁴⁵ We have verified that the low density phase consists of clusters of bonded particles. In the case of $\Delta = 0.2\sigma$ we observe both micelles and vesicles made of a bilayer structure with the attractive hemispheres pointing toward each other. Similar to $\Delta = 0.05\sigma$,³¹ for $\Delta = 0.1\sigma$ we observe micellar clusters, but no vesicles. As both vesicles and wrinkled sheets are based on bilayered structures and absent for $\Delta = 0.1\sigma$, we conclude that this range is too short to stabilize bilayered geometries at low density.

V. JANUS PARTICLES WITH $\Delta = 0.3\sigma$

We now turn our attention to Janus particles with an interaction range $\Delta = 0.3\sigma$. We find (out of a plethora of mechanically stable candidate structures) three different thermodynamically stable crystal phases, see Fig. 6 and Table II,

TABLE II. List of crystal phases for an interaction range of $\Delta = 0.3\sigma$ displaying, $U/N\epsilon$ and $\rho\sigma^3$ for selected $k_B T/\epsilon$, $\beta p\sigma^3$.

$\Delta = 0.3\sigma$				
Phase	$k_B T/\epsilon$	$\beta p\sigma^3/\epsilon$	$U/N\epsilon$	$\rho\sigma^3$
III	0.05	50	-4.75	1.19
IV	0.15	16.7	-4.45	1.16
VI	0.25	10	-3.55	1.09

crystals III, IV, and VI. The resulting phase diagrams in the p - T and ρ - T representations are displayed in Figs. 5(a) and 5(b), respectively.

Crystal III appears at the lowest temperatures, and consists of a body-centered tetragonal (bct) lattice, with the particles oriented in 8 main directions. In Fig. 6 we show both an image of the crystal structure as well as a plot of the distribution of particle directions on the unit sphere, which shows 8 distinct preferred directions. The ground-state interaction energy per particle of crystal III is $U/N\epsilon = -4.75$. Crystal IV appears at higher temperatures. This crystal has a bct lattice as well, but the orientations, if plotted on a unit sphere, are distributed along 4 distinct stripes, see Fig. 6. Crystal IV has an interaction energy per particle

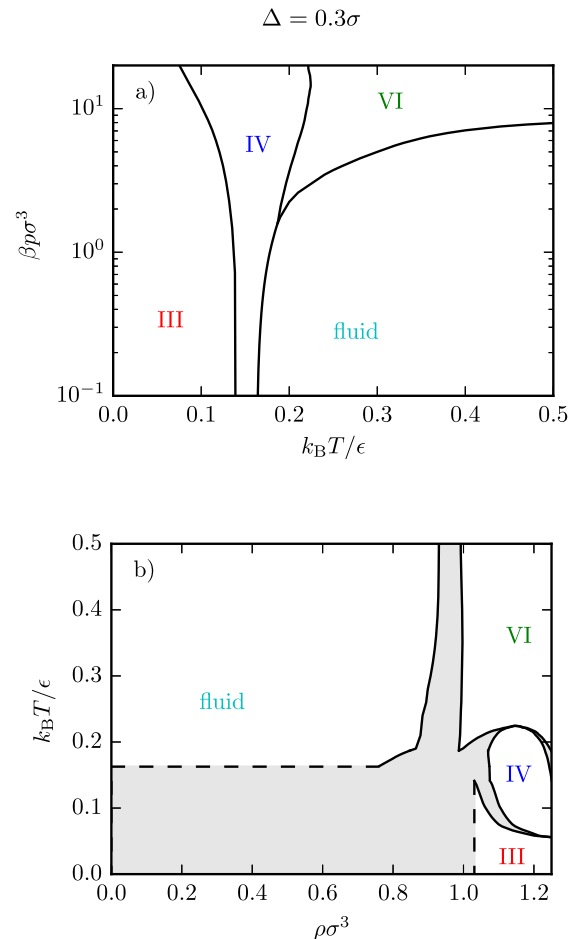


FIG. 5. Phase diagram in (a) p - T and (b) T - ρ plane for the Janus particles with interaction range $\Delta = 0.3\sigma$. Four different phases are stable, III, IV, VI and the fluid. The dashed lines indicate the estimated fluid-crystal coexistence.

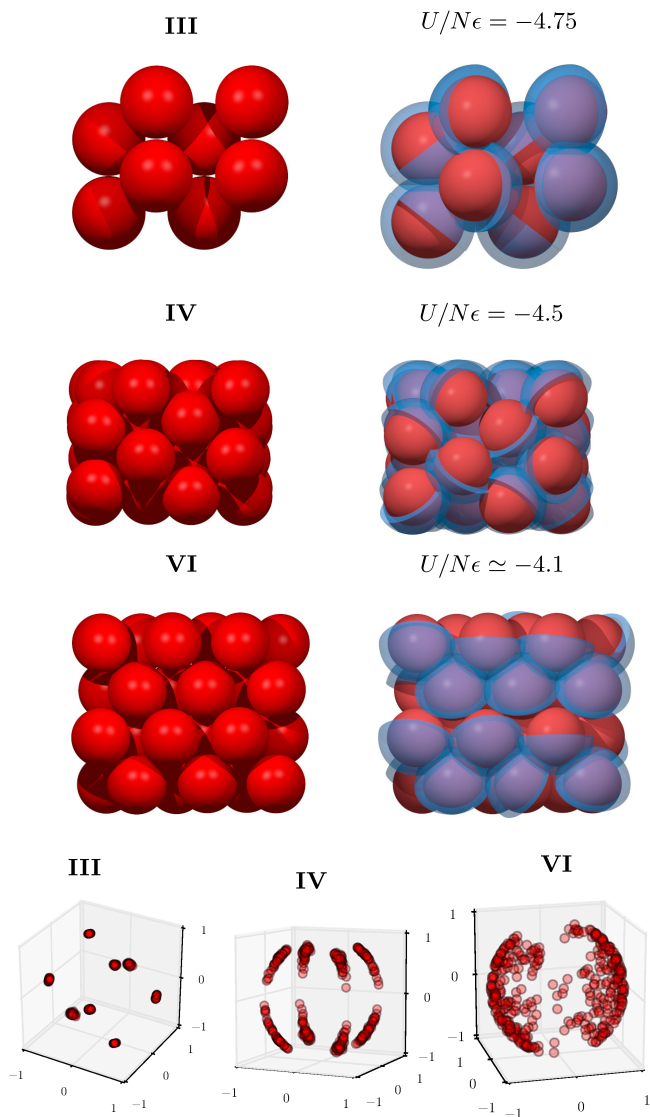


FIG. 6. Stable crystals found for interaction range $\Delta = 0.3\sigma$. On the left the position of the spheres on the lattice is depicted; on the right the particles with their respective bonding volumes (depicted in blue) are shown. The bottom row shows the particle orientations on the unit sphere for each structure.

as $U/N\epsilon = -4.5$. By simulating at different temperatures at constant $p\sigma^3/\epsilon = 2.5$, starting from an initial crystal **IV** structure, a lamellar crystal **VI** spontaneously emerged around $k_B T/\epsilon = 0.24$. Our free-energy calculations confirm that this structure is stable at higher temperatures than crystal **IV**. In crystal **VI**, the particles are on an hcp lattice and are roughly oriented in two main directions, represented by two distinct surfaces on a unit sphere, Fig. 6. This particular orientation distribution increases the rotational freedom of the particles in comparison to crystals **III** and **IV**. However, the interaction energy per particle inside crystal **VI** is considerably higher, about $U/N\epsilon \approx -3.8$.

We note that at lower temperatures, the high-density fluid becomes difficult to equilibrate, making the calculation of the fluid-crystal coexistences with crystals **III** and **IV** computationally too demanding for us to evaluate accurately. At very low T ($k_B T/\epsilon \approx 0.1$) it is, however, possible to estimate the fluid-crystal coexistence assuming that the fluid phase

can be properly modelled as an ideal gas. The fluid-crystal coexistence lines determined this way are reported as dashed lines in Figs. 5(a) and 5(b).

VI. JANUS PARTICLES WITH $\Delta = 0.4\sigma$

We now further increase the interaction range to $\Delta = 0.4\sigma$, and show the phase diagrams in Fig. 7. For this interaction range, five different stable crystal structures are found. The structures and bond orientations of these crystals are given in Fig. 8. Specifically, we detected low energy crystals **VII** and **VIII**, an intermediate crystal structure **IX**, a lamellar crystal in the higher temperature region **X**, and a crystal that is present at high pressures **XI**, see Table III.

We note that the number of candidate crystal structures grows considerably with interaction range, because of the rapid increase of the number of possible bonding configurations (Tables I-IV). For this interaction range, the number of possible bond arrangements is extremely large, due to the ability of the particles to bond with next-nearest neighbours. As a result, the large number of competing crystal structures with approximately the same potential

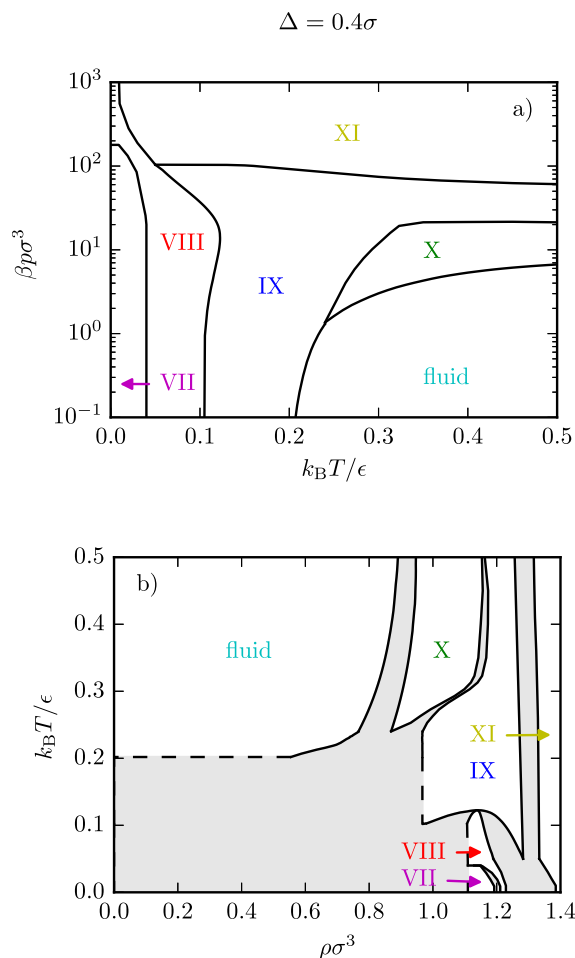


FIG. 7. Equilibrium phase diagram for Janus particles with interaction range $\Delta = 0.4\sigma$ in (a) the T - p and (b) the ρ - T plane. The phase diagram includes five identified stable crystal phases **VII**, **VIII**, **IX**, **X**, and **XI** and a fluid phase. The dashed lines indicate the estimated fluid-crystal coexistence lines.

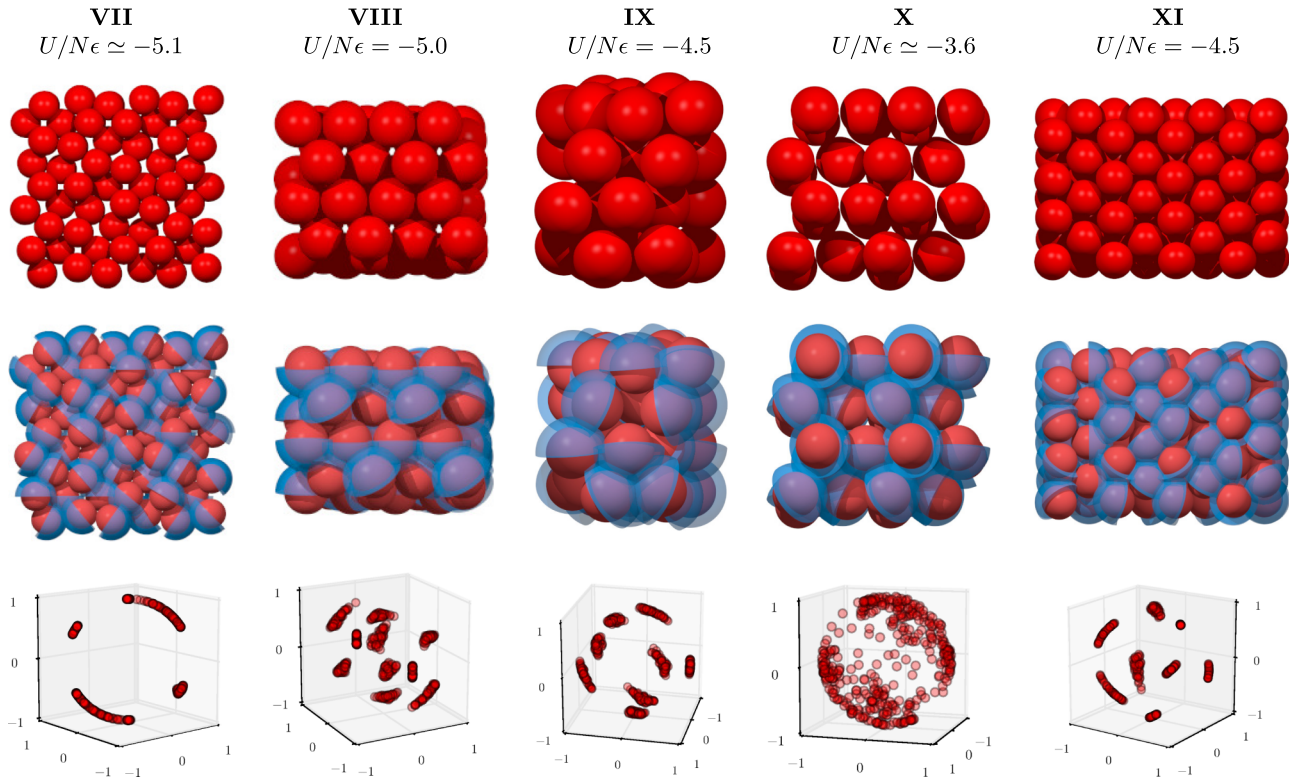


FIG. 8. Stable crystals found for Janus particles with interaction range $\Delta = 0.4\sigma$. Each column is labeled with the crystal name and its energy in the ground state. The first row of images shows the positions of the spheres on the lattice, in the second row the particles with their bonding volumes (shown in blue) are depicted, and the last row shows the particle orientations on the unit sphere.

energy severely hinders the detection of the lowest-energy crystals, which are expected to be stable in low temperature limit. In addition, we found that these structures often required a relatively high number of particles in a unit cell compared to crystals at lower interaction range. To look for low-energy structures, we performed a thorough crystal search using simulations with up to $N = 24$ particles in the variable shape box. For each value of N , we performed at least 100 simulations in parallel. For each simulation, we saved the configurations with the lowest energy. From this, we have identified three distinct low-energy crystals (of which two are thermodynamically stable) with an energy per particle $U/N\epsilon \approx -5$. However, despite the large number of simulations, each of these crystal structures appeared only once as the lowest-energy candidate. This clearly illustrates that for these parameters, the crystals with the lowest interaction energy have a very small probability of being found using the floppy box method.

TABLE III. List of crystal phases for an interaction range of $\Delta = 0.4\sigma$ displaying $U/N\epsilon$ and $\rho\sigma^3$ for selected $k_B T/\epsilon, \beta p\sigma^3$.

$\Delta = 0.4\sigma$				
Phase	$k_B T/\epsilon$	$\beta p\sigma^3$	$U/N\epsilon$	$\rho\sigma^3$
VII	0.01	50	-5.1	1.14
VIII	0.05	10	-5	1.1
IX	0.25	23.2	-4.34	1.18
X	0.35	16.6	-3.58	1.12
XI	0.04	250	-4.5	1.37

These results suggest that there is a high probability that we did not find all relevant low-energy crystal structures, as a result of the inherent difficulty in finding the minimum state in an energy landscape containing many sharp local minima. Additionally, we note that it is unlikely that the lowest-energy structure found for this specific model will be robust to small changes in the interaction potential. Low-energy crystal structures, i.e., crystals with a high number of bonds, often contain particle pairs with relative distances very close to $\sigma + \Delta$ or relative orientations close to $\cos\theta$. For these cases, even a slight change in a bonding distance and/or angle leads to a bond-break. This indeed makes such structures much more difficult to find, as their share of the accessible configurational phase space is very small, while there are many competing local structures with similar energies. Therefore, it can be argued that these crystals are extremely hard to sample and it would be very improbable to find them in experiments.

TABLE IV. List of crystal phases for an interaction range of $\Delta = 0.5\sigma$ displaying $U/N\epsilon$ and $\rho\sigma^3$ for selected $k_B T/\epsilon, \beta p\sigma^3$.

$\Delta = 0.5\sigma$				
Phase	$k_B T/\epsilon$	$\beta p\sigma^3$	$U/N\epsilon$	$\rho\sigma^3$
XII	0.05	20	-6.86	1.05
XIII	0.1	10	-6.25	1.06
XIV	0.3	16.7	-5.05	1.15
XV	0.1	87.5	-5.22	1.34

The lowest-energy crystal we observed is **VII** with an energy $U/N\epsilon \approx -5.1$. Crystal **VII** has a distorted hexagonal lattice, with particle orientations pointing along one plane in four major directions, see Fig. 8. The crystal is stable only in a very small region of the phase diagram, at extremely low temperature. We indeed found that the crystal easily melts when the temperature is increased above $k_B T/\epsilon = 0.05$. The second stable low-energy crystal that we have identified is crystal **VIII**. The crystal consists of alternating layers resolving into an inter-connected lamellar-like structure. The particle orientations are pointing in no less than ten major directions (see Fig. 8), but are restricted to a band around the unit sphere. The crystal has a larger stability field than crystal **VII**, and an energy per particle $U/N\epsilon = -5$.

Beyond the low-energy crystals we identify an intermediate temperature crystal **IX**, with a ground-state interaction energy $U/N\epsilon = -4.5$. This crystal is stable in a significantly larger area of the phase diagram. The particles are orientated in eight directions, see Fig. 8. Upon increasing the temperature, crystal **IX** melts into the next stable crystal **X**, which is a crystal with bond orientations in a lamellar-like fashion as shown in Fig. 8, and relatively few bonds ($U/N\epsilon \approx -3.6$). The last stable crystal we have found for this range is a high pressure hcp crystal labeled **XI**, with a ground-state energy of approximately $U/N\epsilon \approx -4.5$.

The crystal melting densities for $\Delta = 0.4\sigma$ are lower than for the shorter interaction ranges, both due to the longer interaction range and the more open crystal lattices. As for the $\Delta = 0.3\sigma$ case, the free energies and equations of state for the high-density liquid are difficult to calculate at low temperatures. The dashed lines in Fig. 7 indicate estimates for the crystal-fluid coexistence lines based on an ideal gas approximation for the low density fluid.

VII. JANUS PARTICLES WITH $\Delta = 0.5\sigma$

The last investigated interaction range for the Janus particles is $\Delta = 0.5\sigma$. In Fig. 9, we show the full phase diagram, which contains four stable crystal structures, as illustrated in Fig. 10 and Table IV. Of these, the crystal with the lowest energy in the ground state is crystal **XII**, with an interaction energy $U/N\epsilon \approx -6.87$. The particles are on an AA-stacked hexagonal lattice with bonds oriented in the hexagonal plane in six different directions, see Fig. 10. This crystal was found only once from our floppy box simulations out of hundreds of simulations, again illustrating the difficulties with finding low-temperature crystals for long interaction ranges of Janus particles.

At slightly higher temperatures, we find crystal **XIII**, with energy per particle $U/N\epsilon = -6.25$. This structure contains square channels, with the particles oriented in only four directions. At even higher temperatures, we again observe a lamellar structure, crystal **XIV**. However, compared to the lamellar crystals **VIII** and **X** found for $\Delta = 0.4\sigma$, crystal **XIV** is significantly less densely packed, displaying AABB stacking of hexagonal layers as opposed to the pure hollow-site stacking. For $\Delta = 0.5\sigma$, AA stacking permits the formation of bonds with next-nearest neighbours in the adjacent layer,

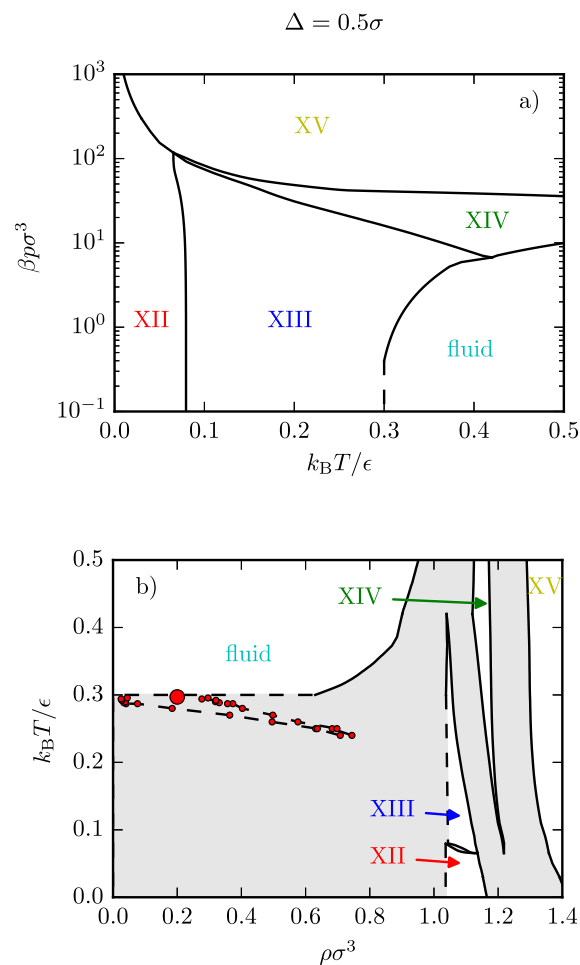


FIG. 9. Equilibrium phase diagram of Janus particles with $\Delta = 0.5\sigma$ in the (a) $T-p$, and (b) $\rho-T$ plane. The dashed lines indicate the estimated fluid-crystal coexistence. Apart from the fluid phase four identified stable crystal phases are present in the phase diagram (**XII**, **XIII**, **XIV**, and **XV**). The red dots indicate the location of the gas-liquid phase separation as estimated in Ref. 45. The dashed lines represent estimates of the fluid-crystal coexistence lines.

leading to a higher number of possible bonds ($U/N\epsilon \approx -5.8$ for crystal **XIV**). Finally, at high pressure we observe crystal **XV**, which consists of an hcp lattice with a complex bonding pattern ($U/N\epsilon \approx -5.28$).

The gas-liquid phase behaviour for this system was previously investigated in Ref. 45, and we include their results in Fig. 9(b). We confirm that the re-entrant gas-liquid coexistence is metastable with respect to the gas-crystal coexistence, similar to what was observed for shorter interaction ranges.¹⁴ The absence of a stable gas-liquid coexistence for any of the investigated interaction ranges up to $\Delta = 0.5\sigma$ is in sharp contrast with earlier observations for particles with isotropic attractions, where interaction ranges on the order of 25% of the particle diameter are typically sufficient to stabilize the gas-liquid transition with respect to crystallization.^{22–25} As suggested in Ref. 45, it is likely that the formation of micelles, which are not mutually attractive, suppresses the gas-liquid phase separation, limiting both the width of the coexistence region and the critical temperature.

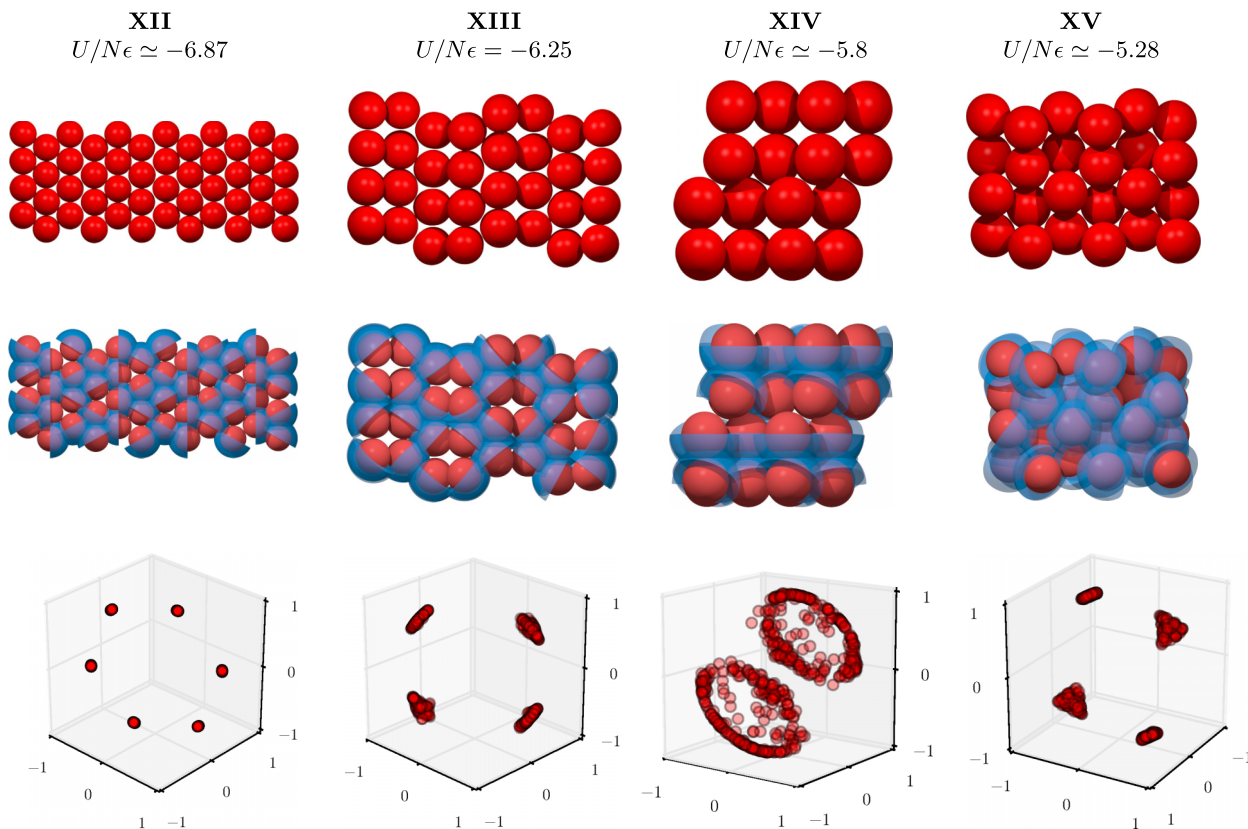


FIG. 10. Identified stable crystals for Janus particles with interaction range $\Delta = 0.5\sigma$. Each column is labeled with the crystal name and its energy in the ground state. The first row of images shows the positions of the spheres on the lattice, in the second row the particles with their bonding volumes (shown in blue) are depicted, and the last row shows the particle orientations on the unit sphere.

VIII. CONCLUSIONS

We have performed a systematic analysis of the effect of the interaction range on the phase diagram of Janus particles, modelled via the Kern-Frenkel potential. Specifically, we studied interaction ranges $\Delta = 0.1\sigma$, 0.3σ , 0.4σ , and 0.5σ , and compare our results to other interaction ranges examined in earlier work. Our results show that for small interaction ranges, the stable crystal structures are limited to those based on close-packed lattices (i.e., hcp and fcc), with different orientational ordering. Thus, apart from stabilizing hcp over fcc in parts of the phase diagram and inducing orientational ordering of the particles, we see no strong changes from the hard-sphere limit ($\Delta \rightarrow 0$). However, when increasing the interaction range ($\Delta \geq 0.2\sigma$), the variety in stable crystal structures starts increasing dramatically. The rich variety of crystal structures includes a wrinkled-sheet structure, bct lattices, various lamellar structures, and AA-stacked hexagonal sheets.

The variety of stable structures at larger interaction ranges is accompanied by a large increase in the number of competing structures with similar energies, which are strongly dependent on the exact range of interaction. This not only makes it significantly more difficult to reliably determine the lowest-energy structures for a given system, but also suggests that spontaneously forming these crystals will be strongly inhibited by kinetic trapping, induced by the large variety of competing alternate structures. Moreover, the strong dependence on interaction details suggests that the

stable structures for the model examined here may not hold for slightly different models, or for real-world realizations of colloidal Janus particles.

Nonetheless, the phase diagrams examined here do show several features which appear to be robust with respect to interaction range. Firstly, we observe no stable gas-liquid coexistence for any of the interaction ranges investigated here. Thus, this feature is likely general for this class of systems, as long as there is no additional source of isotropic attractions. Secondly, we observe bilayered crystals for all interaction ranges $\Delta \geq 0.2\sigma$, including the wrinkled sheets for $\Delta = 0.2\sigma$ and crystals **VI**, **VIII**, **X**, and **XIV**. These structures are typically stable over a large region of the phase diagram, and often can be seen to form spontaneously in the fluid phase. Moreover, these bilayered structures appear mainly at intermediate temperatures, where bond breaking is common and the exact details of the interaction potential are likely to be less important. As a result, we expect this feature to be general for Janus particles as well, which is consistent with the observation of lamellar phases in a variety of simulated and experimental Janus-like systems.^{46–50}

ACKNOWLEDGMENTS

The authors gratefully acknowledge funding from ITN-234810-COMPLOIDS (Z. Preisler), ERC-226207-PATCHYCOLLOIDS (T. Vissers, F. Smallenburg), Stichting voor Fundamenteel Onderzoek der Materie (FOM) (Z. Preisler), FP7-PEOPLE-2013-IEF Marie Curie fellowship

“LivPaC” No. 623364 (T. Vissers), Alexander von Humboldt Foundation (F. Smallenburg), and MIUR-PRIN (F. Sciortino).

- ¹G.-R. Yi, D. J. Pine, and S. Sacanna, *J. Phys.: Condens. Matter* **25**, 193101 (2013).
- ²A. Walther and A. H. E. Müller, *Chem. Rev.* **113**, 5194 (2013).
- ³B. S. Jiang, Q. Chen, M. Tripathy, E. Luijten, K. Schweizer, and S. Granick, *Adv. Mater.* **22**, 1060 (2010).
- ⁴S. Jiang and S. Granick, *Janus Particle Synthesis, Self-Assembly and Applications* (Royal Society of Chemistry, 2012).
- ⁵A. Walther and A. H. E. Müller, *Soft Matter* **4**, 663 (2008).
- ⁶A. B. Pawar and I. Kretzschmar, *Macromol. Rapid Commun.* **31**, 150 (2010).
- ⁷Q. Chen, S. C. Bae, and S. Granick, *Nature* **469**, 381 (2011).
- ⁸Y. Iwashita and Y. Kimura, *Soft Matter* **9**, 10694 (2013).
- ⁹F. Romano and F. Sciortino, *Nat. Mater.* **10**, 171 (2011).
- ¹⁰E. Bianchi, R. Blaak, and C. N. Likos, *Phys. Chem. Chem. Phys.* **13**, 6397 (2011).
- ¹¹S. Roldán-Vargas, F. Smallenburg, W. Kob, and F. Sciortino, *Sci. Rep.* **3** (2013).
- ¹²J. Zhang, E. Luijten, and S. Granick, *Annu. Rev. Phys. Chem.* **66**, 581 (2015).
- ¹³F. Romano, E. Sanz, and F. Sciortino, *J. Chem. Phys.* **132**, 184501 (2010).
- ¹⁴T. Vissers, Z. Preisler, F. Smallenburg, M. Dijkstra, and F. Sciortino, *J. Chem. Phys.* **138**, 164505 (2013).
- ¹⁵F. Romano and F. Sciortino, *Nat. Commun.* **3**, 975 (2012).
- ¹⁶F. Romano, E. Sanz, P. Tartaglia, and F. Sciortino, *J. Phys.: Condens. Matter* **24**, 064113 (2012).
- ¹⁷A. Giacometti, F. Lado, J. Largo, G. Pastore, and F. Sciortino, *J. Chem. Phys.* **132**, 174110 (2010).
- ¹⁸E. Bianchi, J. Largo, P. Tartaglia, E. Zaccarelli, and F. Sciortino, *Phys. Rev. Lett.* **97**, 168301 (2006).
- ¹⁹F. Smallenburg and F. Sciortino, *Nat. Phys.* **9**, 554 (2013).
- ²⁰E. G. Noya, C. Vega, J. P. K. Doye, and A. A. Louis, *J. Chem. Phys.* **132**, 234511 (2010).
- ²¹F. Romano, E. Sanz, and F. Sciortino, *J. Phys. Chem. B* **113**, 15133 (2009).
- ²²S. M. Ilett, A. Orrock, W. Poon, and P. Pusey, *Phys. Rev. E* **51**, 1344 (1995).
- ²³M. Hagen and D. Frenkel, *J. Chem. Phys.* **101**, 4093 (1994).
- ²⁴H. Liu, S. Garde, and S. Kumar, *J. Chem. Phys.* **123**, 174505 (2005).
- ²⁵D. L. Pagan and J. D. Gunton, *J. Chem. Phys.* **122**, 184515 (2005).
- ²⁶S. Jiang, M. J. Schultz, Q. Chen, J. S. Moore, and S. Granick, *Langmuir* **24**, 10073 (2008).
- ²⁷L. Hong, S. Jiang, and S. Granick, *Langmuir* **22**, 9495 (2006).
- ²⁸G. Munaò, Z. Preisler, T. Vissers, F. Smallenburg, and F. Sciortino, *Soft Matter* **9**, 2652 (2013).
- ²⁹Z. Preisler, T. Vissers, F. Smallenburg, G. Munaò, and F. Sciortino, *J. Phys. Chem. B* **117**, 9540 (2013).
- ³⁰T. Vissers, F. Smallenburg, G. Munaò, Z. Preisler, and F. Sciortino, *J. Chem. Phys.* **140**, 144902 (2014).
- ³¹Z. Preisler, T. Vissers, G. Munaò, F. Smallenburg, and F. Sciortino, *Soft Matter* **10**, 5121 (2014).
- ³²W. Bol, *Mol. Phys.* **45**, 605 (1982).
- ³³N. Kern and D. Frenkel, *J. Chem. Phys.* **118**, 9882 (2003).
- ³⁴M. Dijkstra, R. van Roij, and R. Evans, *Phys. Rev. Lett.* **82**, 117 (1999).
- ³⁵R. Roth, R. Evans, and S. Dietrich, *Phys. Rev. E* **62**, 5360 (2000).
- ³⁶C. N. Likos, *Phys. Rep.* **348**, 267 (2001).
- ³⁷C. Vega, E. Sanz, J. L. F. Abascal, and E. G. Noya, *J. Phys.: Condens. Matter* **20**, 153101 (2008).
- ³⁸L. Filion, M. Marechal, B. van Oorschot, D. Pelt, F. Smallenburg, and M. Dijkstra, *Phys. Rev. Lett.* **103**, 188302 (2009).
- ³⁹E. Bianchi, G. U. Doppelbauer, L. Filion, M. Dijkstra, and G. Kahl, *J. Chem. Phys.* **136**, 214102 (2012).
- ⁴⁰D. A. Kofke, *J. Chem. Phys.* **98**, 4149 (1993).
- ⁴¹F. Sciortino, A. Giacometti, and G. Pastore, *Phys. Chem. Chem. Phys.* **12**, 11869 (2010).
- ⁴²Q. Chen, E. Diesel, J. K. Whitmer, S. C. Bae, E. Luijten, and S. Granick, *J. Am. Chem. Soc.* **133**, 7725 (2011).
- ⁴³Q. Chen, S. C. Bae, and S. Granick, *J. Am. Chem. Soc.* **134**, 11080 (2012).
- ⁴⁴Y. Iwashita and Y. Kimura, *Soft Matter* **10**, 7170 (2014).
- ⁴⁵F. Sciortino, A. Giacometti, and G. Pastore, *Phys. Rev. Lett.* **103**, 237801 (2009).
- ⁴⁶A. K. Khandpur, S. Foerster, F. S. Bates, I. W. Hamley, A. J. Ryan, W. Bras, K. Almdal, and K. Mortensen, *Macromolecules* **28**, 8796 (1995).
- ⁴⁷J. Hu, S. Zhou, Y. Sun, X. Fang, and L. Wu, *Chem. Soc. Rev.* **41**, 4356 (2012).
- ⁴⁸T. Higuchi, A. Tajima, K. Motoyoshi, H. Yabu, and M. Shimomura, *Angew. Chem.* **120**, 8164 (2008).
- ⁴⁹D. J. Beltran-Villegas, B. A. Schultz, N. H. Nguyen, S. C. Glotzer, and R. G. Larson, *Soft Matter* **10**, 4593 (2014).
- ⁵⁰V. Percec, D. A. Wilson, P. Leowanawat, C. J. Wilson, A. D. Hughes, M. S. Kaucher, D. A. Hammer, D. H. Levine, A. J. Kim, F. S. Bates *et al.*, *Science* **328**, 1009 (2010).